

Characterization of methanol as a magnetic field tracer in star-forming regions

Boy Lankhaar* and Wouter Vlemmings

*Department of Space, Earth and Environment,
Chalmers University of Technology,
Onsala Space Observatory, 439 92 Onsala, Sweden*

Gabriele Surcis

*Joint Institute for VLBI ERIC, Postbus 2,
7990 AA Dwingeloo, The Netherlands and
INAF, Osservatorio Astronomico di Cagliari Via della Scienza 5, I-09047 Selargius, Italy*

Huib Jan van Langevelde

*Joint Institute for VLBI ERIC, Postbus 2,
7990 AA Dwingeloo, The Netherlands and
Sterrewacht Leiden, Leiden University,
Postbus 9513, 2330 RA Leiden, the Netherlands*

Gerrit C. Groenenboom and Ad van der Avoird

*Theoretical Chemistry, Institute for Molecules and Materials,
Radboud University, Heyendaalseweg 135,
6525 AJ Nijmegen, The Netherlands*

(Dated: February 19, 2018)

* boy.lankhaar@chalmers.se

Magnetic fields play an important role during star formation[1]. Direct magnetic field strength observations have proven specifically challenging in the extremely dynamic protostellar phase[2–4]. Because of their occurrence in the densest parts of star forming regions, masers, through polarization observations, are the main source of magnetic field strength and morphology measurements around protostars[2]. Of all maser species, methanol is one of the strongest and most abundant tracers of gas around high-mass protostellar disks and in outflows. However, as experimental determination of the magnetic characteristics of methanol has remained largely unsuccessful[5], a robust magnetic field strength analysis of these regions could hitherto not be performed. Here we report a quantitative theoretical model of the magnetic properties of methanol, including the complicated hyperfine structure that results from its internal rotation[6]. We show that the large range in values of the Landé g-factors of the hyperfine components of each maser line lead to conclusions which differ substantially from the current interpretation based on a single effective g-factor. These conclusions are more consistent with other observations[7, 8] and confirm the presence of dynamically important magnetic fields around protostars. Additionally, our calculations show that (non-linear) Zeeman effects must be taken into account to further enhance the accuracy of cosmological electron-to-proton mass ratio determinations using methanol[9–12].

The presence of a magnetic field within an astrophysical maser produces partially polarized radiation. Linear polarization provides information on the magnetic field direction, while the magnetic field strength can be determined by comparing the field-induced frequency shifts between left- and right-circularly polarized maser emission. Extraction of the relevant information from polarized maser spectra requires knowledge of the Zeeman parameters which describe the response of the maser molecule/atom to a magnetic field. These Zeeman parameters are known for maser molecules such as OH, H₂O, and SiO, but not for methanol.

Various torsion-rotation transitions of methanol have been observed as astrophysical masers. It has long been known that these transitions have a hyperfine structure, but only recently has an accurate model of this structure been presented[6]. It was shown that the so-called torsional motion of CH₃OH about the CO bond drastically complicates the

hyperfine interactions and that ‘spin-torsion’ terms occur in addition to the usual ‘spin-rotation’ and spin-spin coupling terms. The magnetic moments that produce the hyperfine structure also interact with an external magnetic field, a Zeeman effect. Here, we extend the model of methanol’s hyperfine structure with the Zeeman interactions. We quantitatively determined all the relevant coupling parameters, including effects from the torsional motion, by quantum-chemical *ab initio* calculations and an estimate of the torsional Zeeman effect based on experimental results[13]. With this model, we can determine the Zeeman splitting of the hyperfine states within all the known methanol maser transitions.

Zeeman interactions are usually described in a first-order approximation by the Landé g-factor. In methanol, each torsion-rotation transition is actually split into a number of transitions between individual hyperfine levels of the upper and lower torsion-rotation states (Figure 1). The Landé g-factors calculated for the different hyperfine transitions differ strongly and, even though these transitions cannot be individually resolved in the observed maser spectra, we will show that this is important for the interpretation of the measured polarization effects. Furthermore, we found that in several cases the energy gaps between hyperfine levels are so small that hyperfine states with different total angular momenta F get mixed even by a weak magnetic field. In such cases, the first-order approximation for the Zeeman interactions breaks down, and the Zeeman splittings depend non-linearly on the magnetic field strength (Figure 2). Also the Einstein A-coefficients of transitions between two hyperfine levels become magnetic-field dependent quantities in these cases (Supplementary Figure 2). This behavior has not previously been seen in Zeeman interactions for non-paramagnetic molecules, and is therefore not accounted for in current maser-polarization theory[14, 15].

To apply our results to maser-polarization measurements, we must consider hyperfine-specific effects in the maser action. The individual hyperfine lines are not spectrally resolved, but the maser action can favor specific hyperfine transitions by the following mechanisms: i) varying radiative rates for stimulated emission (see the Einstein coefficients of the various hyperfine components within a torsion-rotation line (Supplementary Information)). ii) kinematic effects, when there are two maser clouds along the line of sight with different velocities, such that a hyperfine transition in the foreground cloud amplifies emission from a different hyperfine transition in the background cloud[16], iii) population inversion of the levels involved in maser action is preceded by collisional and radiative de-excitation of higher

torsion-rotation levels[17], with rate coefficients that are hyperfine-state specific[18]. The latter effect has been overlooked in current maser excitation models[17], thus no quantitative information is available. To obtain a qualitative understanding, we considered the relative hyperfine-specific collisional and radiative rates within a torsion-rotation transition. We find for de-excitation collisions of methanol with helium atoms (equation (8)), and for radiative emission (equation (12)), that the hyperfine levels with the highest F quantum number have the largest relative de-excitation rate coefficients.

Up to now, methanol maser circular polarization observations have been made for the 6.7 GHz ($5_{15} A_2 \rightarrow 6_{06} A_1$)[2, 19], 44 GHz ($7_{07} A_2 \rightarrow 6_{16} A_1$)[4, 20] and 36 GHz ($4_{-1} E \rightarrow 3_0 E$)[3] torsion-rotation transitions. As the magnetic characteristics of methanol were not known, (hyperfine unspecific) estimates of the Zeeman parameters were used. In the following, we will re-analyze some of the observations using our calculated Zeeman parameters (Supplementary Table 1). We take into account that within a torsion-rotation transition the various hyperfine transitions have different Landé g -factors (Supplementary Tables 2-18) and that the maser action can be hyperfine-state specific.

We begin with the circular-polarization observations of class II 6.7 GHz methanol masers occurring in protostellar disks. We assume that the transition with the largest Einstein coefficient for stimulated emission, the $F = 3 \rightarrow 4$ transition (see Figure 1 and Supplementary Table 3), will be favored and that the maser action is limited to this transition. Then, the Zeeman-splitting coefficient α_Z (related to the Landé g -factor g_l as $\alpha_Z = \mu_N g_l$ with μ_N being the nuclear magneton) of the maser-transition will be $\alpha_Z = -1.135 \text{ Hz mG}^{-1}$, which is 10 times larger than the value currently used for magnetic field estimates[2, 5]. In the methanol maser regions probed by these class II masers, with an H_2 number density of $n_{\text{H}_2} \approx 10^8 \text{ cm}^{-3}$ [17], application of our new results to a large sample of maser observations[2] indicates an average field strength of $\langle |B| \rangle \approx 12 \text{ mG}$. If, instead of by the $F = 3 \rightarrow 4$ hyperfine transition, the polarization is caused by a combination of hyperfine components or by any of the other components, the derived magnetic field strength would be higher. Including all hyperfine components would result in an average $\alpha_Z \approx 0.17 \text{ Hz mG}^{-1}$ and $\langle |B| \rangle \approx 80 \text{ mG}$. This is significantly larger than expected based on OH masers observed at similar densities[7, 8]. The results based on the $F = 3 \rightarrow 4$ transition are in good agreement with OH-maser polarization observations[7, 8], as well as with the extrapolated magnetic field vs. density relation $B \propto n^{1/2}$ [21, 22]. This indicates, as already suggested by linear polarization

TABLE I: Zeeman splitting parameters α_Z (in Hz mG⁻¹) for the strongest $\Delta F = \Delta J$ transitions of the investigated maser lines. The ranges of the quantum number F for states of A symmetry are explained in the caption of Figure 1. Torsion-rotation states of E symmetry state have nuclear spin $I = 0$ and 1, so that for $J \geq 1$ there are hyperfine states with $F = J$ and $F = J \pm 1$. Each torsion-rotation function of E symmetry yields two sets of hyperfine states of overall symmetry A_1 and A_2 [6]. In this table, the hyperfine lines for each $J \rightarrow J'$ torsion-rotation transition are indicated by their initial F value, relative to the corresponding J value. For A -symmetry a single transition is associated with each $F = J \pm 2$ and two transitions with each $F = J, J \pm 1$. For E -symmetry two transitions $A_1 \rightarrow A_2$ and $A_2 \rightarrow A_1$ are associated with each $F = J \pm 1$ and four transitions with $F = J$.

	$F = J - 2$	$F = J - 1$	$F = J$	$F = J + 1$	$F = J + 2$
$5_{15} A_2 \rightarrow 6_{06} A_1$ (6.7 GHz)	-1.135	-0.516 -0.467	-0.127 0.002	0.224 0.261	0.472
$7_{07} A_2 \rightarrow 6_{16} A_1$ (44 GHz)	-0.920	-0.436 -0.403	-0.016 -0.108	0.207 0.203	0.413
$4_{-1} E \rightarrow 3_0 E$ (36 GHz)		-0.704	-0.075 0.056	0.424	
		-0.729	-0.274 0.174	0.486	

studies[19, 23], that methanol masers probe the large scale magnetic field around massive protostars. Reversely, extending the magnetic field vs. density relation by almost two orders of magnitude in density provides important constraints on the theory of massive star formation, as it implies that the magnetic energy density remains important up to densities of $n_{\text{H}_2} \approx 10^9 \text{ cm}^{-3}$. The conclusions are also supported by a more specific study of Cepheus A HW2[23] (Figure 3), where our reinterpretation confirms a slightly supercritical maser region, giving rise to magnetically regulated accretion towards the disc of Cepheus A HW2.

Polarization observations of class I methanol masers in the outflows of massive star-forming regions have been made for the 36 GHz and 44 GHz torsion-rotation transitions. In both lines the individual hyperfine transitions are clustered in two groups, which gives rise to a doublet structure in the spectra[6]. Considering kinematic effects favoring one of the two peaks and selecting from this peak the transition with the largest coefficient for stimulated emission, we assume that the $F = 3 \rightarrow 2$ (36 GHz) and $F = 5 \rightarrow 4$ (44 GHz) hyperfine lines are favored and that the maser action is limited to these transitions. Then,

the Zeeman-splitting coefficients of the maser-transitions will be $\alpha_Z = -0.704 \text{ Hz mG}^{-1}$ for the 36 GHz line and $\alpha_Z = -0.920 \text{ Hz mG}^{-1}$ for the 44 GHz line (Supplementary Tables 10 and 4). The observed class I methanol masers are expected to occur in shocked regions of the outflows at densities of an order of magnitude lower in comparison to class II masers[24]. The Zeeman splitting of the 36 GHz and 44 GHz lines was found to be on the order of several tens of Hz[3, 4, 20]. Using our analysis, this would indicate magnetic field strengths of 20 – 75 mG. Since, class I masers are shock excited, shock compression is expected to increase the magnetic field strength. For the outflow velocities in the class I maser regions, a pre-shock magnetic field as observed in the OH maser regions ($\approx 5 \text{ mG}$) will be amplified to $> 20 \text{ mG}$, consistent with the observations. We thus suggest that class I methanol maser polarization observations provide important information on the shock conditions of proto-stellar outflows.

Our results also suggest an explanation for a surprising feature observed in both Class II (6.7 GHz) and Class I (44 GHz) masers. Observations have shown reversals in the sign of polarization over areas of small angular extent in the sky (6.7 GHz, see Figure 3 and 44 GHz, see Figure 2 in Ref. [20]). Such reversals have usually been interpreted as a change in field direction. However, reversals on au-scales would be surprising if one considers the agreement between the fields probed by methanol masers and dust emission[25]. A more plausible explanation favored by our results is that in the masers with opposite signs of polarization, the masing process itself is due to the dominance of different hyperfine transitions. If we assume for the 6.7 GHz spectrum that for the ‘recalcitrant’ maser the $F = 7 \rightarrow 8$ hyperfine transition is favored by kinematic effects, instead of the $F = 3 \rightarrow 4$ transition for the other masers, we find a magnetic field comparable to the result from other masers along the line of sight (Figure 3). For the 44 GHz maser, if we assume the $F = 8 \rightarrow 7$ transition to be favored for the ‘recalcitrant’ maser instead of the $F = 5 \rightarrow 4$ transition for the other maser, we also get Zeeman-splitting coefficients with opposite signs and we find similar magnetic fields of $\approx 50 \text{ mG}$ from both masers composing the signal. We thus find that an alternative preferred hyperfine transition in the maser action is able to explain opposite circular polarization along the line of sight, and obtain magnetic fields comparable with the results from other masers that trace similar areas around the protostar.

Our model is also important for the study of methanol maser absorption in red-shifted cosmological sources. Methanol’s high sensitivity to variation of the electron-to-proton mass

ratio in the torsion-rotational structure is enhanced by its torsional motion[11]. Extra-galactic absorption measurements of the $3_{-1} E \rightarrow 2_0 E$, 12.2 GHz transition have been used to provide the strongest constraints on the time variation of the electron-to-proton mass ratio[9, 10]. Recently, measurements with a high spatial resolution have been able to selectively observe methanol absorption in an extra-galactic cold core[26]. Hyperfine effects shift the center of torsion-rotation lines, which is an effect not accounted for in the current torsion-rotation fitting Hamiltonian[27] from which the parameters are used in determination of the sensitivity coefficients[11, 28]. Also, in cold extra-galactic regions, temperature broadening effects are smaller than the hyperfine splittings, which could be resolved with a sufficiently high spectral resolution. Furthermore, in regions with strong magnetic fields (> 30 mG), this structure will be affected by Zeeman effects. These effects should be included in the error-accounting of the constraints to the time variation of the electron-to-proton mass ratio.

Theoretical modeling of (non-linear) Zeeman effects for other molecular species such as HCN and H₂CO can also be done according to the theory presented here. The same care should be taken in the assessment of Zeeman effects in radical species, where the magnetic field can mix fine-structure states, which is analogous to hyperfine mixing. This will be particularly important for CCS[29, 30], for which the Zeeman characteristics are still poorly known, but which will be one of the prime molecules for Zeeman studies with the Square Kilometer Array.

METHODS

We theoretically modeled the response of methanol to weak magnetic fields by the addition of magnetic field (Zeeman) interactions to the model for methanol’s hyperfine structure from Ref. [6]. Here, we will briefly revisit methanol’s hyperfine structure and describe the relevant Zeeman interactions. Next, we will detail the computational methods used to obtain the molecule-specific coupling parameters. Finally, we describe the methods used to compute the magnetic field dependent spectrum of methanol.

Hyperfine structure

The elucidation of methanol’s hyperfine structure has been a challenging problem. The CH_3 -group in methanol can easily rotate with respect to the OH-group, which leads to an extension of the usual rigid-rotor hyperfine Hamiltonian with nuclear spin-torsion interactions[31]. In contrast with the nuclear spin-rotation coupling parameters, for which the *ab-initio* calculated values have recently been experimentally confirmed[32], the torsional hyperfine coupling parameters cannot be obtained from quantum chemical *ab initio* calculations [6, 33]. Experiments probing the hyperfine structure of methanol have proven difficult to interpret, because the hyperfine transitions cannot be individually resolved. Lankhaar *et al.*[6] revised the derivation of a Hamiltonian which includes the torsional hyperfine interactions and obtained the coupling parameters in this Hamiltonian from both *ab initio* calculations and experimental data[31, 33]. The hyperfine spectra of methanol calculated from this Hamiltonian agree well with the spectra observed for several torsion-rotation states of both *A*- and *E*-symmetry. In our present calculations of the Zeeman interactions of methanol in external magnetic fields we start from this hyperfine Hamiltonian. For a detailed description, see Ref. [6].

Zeeman Hamiltonian

Zeeman interactions are governed by the same magnetic moments that determine the hyperfine structure, interacting with an external magnetic field \mathbf{B} . For a closed-shell diamagnetic molecule as methanol three contributions are important, from the overall rotation, the internal rotation or torsion, and the nuclear spins. The most abundant ^{12}C and ^{16}O nuclei have spin zero, so the nuclear spin of methanol, CH_3OH , comes from the three protons in the CH_3 group and the proton in the OH group. As it was derived in Appendix A of Ref. [6] for the corresponding hyperfine Hamiltonian, the rotational Zeeman Hamiltonian

$$\hat{H}_{\text{BR}} = -\frac{\mu_N}{\hbar} \mathbf{B} \cdot \mathbf{g}(\gamma) \hat{\mathbf{J}} + \frac{\mu_N}{\hbar} f \mathbf{B} \cdot \mathbf{g}(\gamma) \boldsymbol{\lambda} \left(\hat{p}_\gamma - \boldsymbol{\rho} \cdot \hat{\mathbf{J}} \right), \quad (1)$$

depends not only on the overall rotation angular momentum $\hat{\mathbf{J}}$, but also on the torsional angular momentum $\hat{p}_\gamma = (\hbar/i)\partial/\partial\gamma$. μ_N is the nuclear magneton. The coupling tensor \mathbf{g} has the same form as for semi-rigid molecules, but for molecules with internal rotation it depends on the torsional angle γ . The unit vector $\boldsymbol{\lambda}$ describes the direction of the internal

rotation axis in the principal axes frame of the molecule and $\boldsymbol{\rho} = \mathbf{I}^{-1}\mathbf{I}^{\text{CH}_3}\boldsymbol{\lambda}$, where \mathbf{I} is the total inertia tensor and \mathbf{I}^{CH_3} the inertia tensor of the CH_3 group. The dimensionless factor f depends on the ratio of the moments of inertia of the OH frame and the rotating CH_3 top about the torsional axis[6].

In addition, we must account for torsional Zeeman effects. Similarly to the torsional hyperfine Hamiltonian \hat{H}_{ST} in Ref. [6], the torsional Zeeman Hamiltonian

$$\hat{H}_{\text{BT}} = -\frac{\mu_N}{\hbar} f \mathbf{B} \cdot \mathbf{b}(\gamma) \left(\hat{p}_\gamma - \boldsymbol{\rho} \cdot \hat{\mathbf{J}} \right), \quad (2)$$

with the coupling vector $\mathbf{b}(\gamma)$, not only contains the torsional angular momentum operator \hat{p}_γ , but also the total angular momentum $\hat{\mathbf{J}}$. By absorbing the second term of \hat{H}_{BR} in equation (1) into equation (2), the remaining rotational Zeeman Hamiltonian obtains the usual form it has for a semi-rigid molecule, and we obtain an effective torsional Hamiltonian \hat{H}_{BT} with $\mathbf{b}(\gamma)$ replaced by

$$\mathbf{b}'(\gamma) = \mathbf{b}(\gamma) - \mathbf{g}(\gamma)\boldsymbol{\lambda}, \quad (3)$$

Finally, the intrinsic magnetic moments of the protons $K = 1, 2, 3$ in the CH_3 group and proton $K = 4$ in the OH group interact with the magnetic field

$$\hat{H}_{\text{BS}} = -\frac{\mu_N}{\hbar} g_p \sum_K \mathbf{B} \cdot \hat{\mathbf{I}}_K, \quad (4)$$

where g_p is the proton g-factor. The total Zeeman Hamiltonian is a sum of the rotational, torsional, and nuclear spin Zeeman terms

$$\hat{H}_{\text{Zeeman}} = \hat{H}_{\text{BR}} + \hat{H}_{\text{BT}} + \hat{H}_{\text{BS}}. \quad (5)$$

Coupling tensors

The response of methanol to magnetic fields is theoretically modeled by including the coupling of the relevant angular momenta—the rotational angular momentum, the torsional momentum, and the nuclear spin angular momentum—to the magnetic field vector. The couplings between these angular momentum operators and the magnetic field involve a rank-2 coupling tensor and a coupling vector. This coupling tensor and vector are specific for methanol. The derivation of the hyperfine coupling tensors is given in Ref. [6], and of the Zeeman coupling tensors in the Supplementary Information. This subsection describes the methods used to evaluate all coupling parameters.

Rotational g-tensor

Rotational Zeeman effects are represented by the molecule-specific g-tensor, which for rigid non-paramagnetic molecules has been extensively studied experimentally for its valuable information on the electronic structure[34–37]. Nowadays, quantum chemical calculations[38, 39] are able to reproduce these experiments with high accuracy. The rotational g-tensor $\mathbf{g}(\gamma)$ can be obtained from *ab initio* electronic structure calculations with the program package CFOUR[40]. We carried out calculations with CFOUR at the coupled-cluster level of theory including single and double excitations with perturbative addition of the triples contribution [CCSD(T)], in an augmented triple-zeta correlation-consistent (aug-cc-pVTZ) basis set[41]. The geometry of methanol was optimized at this level, which yields bond lengths OH, CO, and CH of 0.956, 1.427, and 1.096 Å, respectively, bond angles COH and OCH of 108.87° and 109.91°, and a torsional HOCH angle of 180°. The electronic contributions to $\mathbf{g}(\gamma)$ were calculated at the same level of theory for 13 equidistant values of the torsional angle γ by keeping the HOC fragment fixed and rotating the CH₃ group over these angles about the OC bond axis. The nuclear contribution to the tensor $\mathbf{g}(\gamma)$ was also given by CFOUR, but was also calculated directly from the nuclear coordinates. Because of methanol’s symmetry, we could fit our *ab initio* calculated values for the rotational $\mathbf{g}(\gamma)$ -tensor elements to $\sum_n a_{3n} \cos(3n\gamma)$ or $\sum_n a_{3n} \sin(3n\gamma)$ functions of the internal rotation angle. The expansion coefficients, a_{3n} , are listed in Supplementary Table 1.

Torsional b-vector

Torsional Zeeman interactions are represented by the molecule-specific b-vector (Supplementary equations (16) and (21)). The calculation of the electronic contribution to the b-vector has not been implemented in the available quantum-chemical program packages. In order to estimate the torsional Zeeman effects in methanol, we compare its internally rotating CH₃-group to the CH₃-groups of nitromethane and methyl-boron-difluoride, of which the torsional Zeeman effect has been investigated experimentally[13, 42].

The torsional Zeeman coupling vectors of nitromethane and methyl-boron-difluoride were determined to be $\mathbf{b} = g_\gamma \boldsymbol{\lambda}$, with $g_\gamma = 0.347$ and 0.3415, respectively. In these molecules the unit vector $\boldsymbol{\lambda}$ that defines the direction of the internal rotation axis lies along the main prin-

principal axis. The small difference in the g -values of these two molecules was explained by the electron drainage from the CH_3 -groups by the attached functional group (see Supplementary Information). This electron drainage can be estimated from the partial atomic charges given by a Mulliken population analysis[43]. We calculated Mulliken populations of the CH_3 -groups of nitromethane and methyl-boron-difluoride at the CCSD(T) level in an aug-cc-pVDZ basis, at their *ab initio* optimized geometries, and found that $P_{\text{CH}_3(-\text{NO}_2)} = 8.714$ and $P_{\text{CH}_3(-\text{BF}_2)} = 9.232$. The Mulliken population of the CH_3 -group in methanol was computed at the same level and found to be $P_{\text{CH}_3(-\text{OH})} = 8.737$. Then, we obtained the \mathbf{b} -vector of methanol by interpolation as $\mathbf{b} = g_\gamma \boldsymbol{\lambda}$, with $g_\gamma = 0.3468$, see Supplementary Table 1. In this estimate of \mathbf{b} , we have assumed that it is independent of the internal rotation angle γ and is parallel to $\boldsymbol{\lambda}$. The latter assumption holds only when $\boldsymbol{\lambda}$ is directed along one of the principal axes, which is almost the case for methanol[6, 27].

Matrix elements and spectrum

With the knowledge of the coupling tensors $\mathbf{g}(\gamma)$ and $\mathbf{b}(\gamma)$ in the Zeeman Hamiltonian of equation (5) and the use of the hyperfine Hamiltonian from Ref. [6] we computed the magnetic field dependence of the hyperfine levels. The total Hamiltonian is diagonalized in the basis $|(I_{123}, I_4)I, J\rangle FM_F\rangle$ obtained by coupling the eigenfunctions of the torsion-rotation Hamiltonian[27] with the nuclear spin functions $|(I_{123}, I_4)I\rangle$ of the appropriate symmetry, defined in Sec. IIC of Ref. [6]. The hyperfine interactions couple the total nuclear spin I with the torsion-rotation angular momentum J to a total angular momentum F , with projection M_F on the space-fixed z -axis chosen along the magnetic field direction \mathbf{B} . When the external magnetic field is included, only M_F remains a good quantum number. Hyperfine states with different F may get mixed, which happens to a substantial extent when there is a small energy gap between the hyperfine levels.

The torsion-rotation wave functions[27] have quantum numbers v_τ , J , K_a and symmetry A or E . For symmetries A and E , the nuclear spin basis has $I_{123} = 3/2$ and $1/2$, respectively, see Sec. IIC in Ref. [6]. The energy gaps between torsion-rotation states are typically on the order of a few GHz, while the hyperfine and Zeeman interactions in methanol (for fields $B < 10$ G) amount to about 10 kHz. Hence, we may restrict our basis to a single value of v_τ and J and derive an effective Zeeman Hamiltonian of which the matrix elements are more

easily evaluated (Supplementary Information).

The matrix of the total Zeeman plus hyperfine Hamiltonian over the hyperfine basis with quantum numbers F, M_F [6] is evaluated and diagonalized. This yields the splitting of the hyperfine levels into $2F + 1$ sublevels, with M_F as the only good quantum number. Intensities and Einstein A-coefficients for transitions between the individual hyperfine levels are obtained with the procedures described in Ref. [6].

Hyperfine-state resolved de-excitation

It is emphasized in the letter that the Landé g-factors of the different hyperfine components of each torsion-rotation transition vary over a large range of values. It is therefore important to know the populations of the individual hyperfine levels of the torsion-rotation states involved in the methanol maser action. This maser action is preceded by collisional and radiative de-excitation of higher torsion-rotation levels. Here, we derive formulas to estimate relative hyperfine-state-specific collisional and radiational de-excitation rate coefficients.

Hyperfine-state resolved collisional rate coefficients

Hyperfine splittings are negligible with respect to the collision energy, so to an excellent approximation the collision dynamics depends only on the scattering conditions and on the torsion-rotation structure of the molecule, and is not affected by hyperfine effects[18, 44]. As a consequence, obtaining hyperfine-state-specific $F \rightarrow F'$ transition rate coefficients from the usual rate coefficients for rotationally inelastic $J \rightarrow J'$ collisions requires only the use of an appropriate basis in which the angular momentum J is coupled with the total nuclear spin I to total angular momentum F [18, 45].

Davis[46] analyzed the collision dynamics of a structureless atom (such as helium) and a molecule with one internal rotation (as methanol), using a simple torsion-rotation model and neglecting the molecule's vibrational modes. The presence of the torsional modes leads to additional inelastic scattering processes, but the angular momentum algebra in the expressions for the scattering amplitudes and cross sections are similar for collisions with methanol and with diatomic molecules. The methanol symmetric rotor quantum number K_a and tor-

sional quantum numbers v_τ and σ only play a spectator role with regard to the angular momentum (re-)coupling[46].

To perform coupled-channel calculations for collisions of methanol with helium in a hyperfine basis would exceed the scope of this letter. Rather, we want to get an idea of the general trends of the hyperfine inelastic scattering rates with respect to the corresponding rotational rates. To this end, we use a formalism that relates the torsion-rotation inelastic scattering cross sections to hyperfine-state-specific cross sections. This is most conveniently done by representing the cross sections in terms of tensor opacities[44, 46]

$$\sigma_{(K_a\sigma v_\tau)J \rightarrow (K'_a\sigma'v'_\tau)J'} = \frac{\pi}{[J]k_{(K_a\sigma v_\tau)J}^2} \sum_L P^{(L)}((K_a\sigma v_\tau)J \rightarrow (K'_a\sigma'v'_\tau)J'), \quad (6)$$

where $k_{(K_a\sigma v_\tau)J}$ is the wave vector dependent on the collision energy and the torsion-rotation energy of the initial state, L is the rank of the tensor opacity $P^{(L)}$, and the square bracket notation designates $[J] = 2J + 1$. Recoupling the nuclear-spin free opacity to the hyperfine-state-specific opacity yields[44]

$$P^{(L)}((K_a\sigma v_\tau)[JI]F \rightarrow (K'_a\sigma'v'_\tau)[J'I]F') = [F][F'] \left\{ \begin{matrix} J & J' & L \\ F' & F & I \end{matrix} \right\}^2 P^{(L)}((K_a\sigma v_\tau)J \rightarrow (K'_a\sigma'v'_\tau)J'). \quad (7)$$

The expression in curly brackets is a $6j$ -symbol. Substitution of this result into equation (6), yields the hyperfine-state-specific collisional cross sections

$$\begin{aligned} \sigma_{(K_a\sigma v_\tau)[JI]F \rightarrow (K'_a\sigma'v'_\tau)[J'I]F'} &= \frac{\pi}{k_{(K_a\sigma v_\tau)J}^2 [F]} \sum_L P^{(L)}((K_a\sigma v_\tau)[JI]f \rightarrow (K'_a\sigma'v'_\tau)[J'I]F') \quad (8) \\ &= \frac{\pi [F']}{k_{(K_a\sigma v_\tau)J}^2} \sum_L \left\{ \begin{matrix} J & J' & L \\ F' & F & I \end{matrix} \right\}^2 P^{(L)}((K_a\sigma v_\tau)J \rightarrow (K'_a\sigma'v'_\tau)J'). \end{aligned}$$

The triangular condition imposes the constraint $|J - J'| \leq L \leq J + J'$. Each of these values of L contributes to the total hyperfine-state-specific collisional rates. Except for very low collision energies where resonances may occur, which are not important at the methanol maser conditions, the largest contribution comes from $L = |\Delta J|$. Considering this contribution only would directly relate the hyperfine-state-specific rate with the rotational rate[45]

$$\sigma_{(K_a\sigma v_\tau)[JI]F \rightarrow (K'_a\sigma'v'_\tau)[J'I]F'} = [J][F'] \left\{ \begin{matrix} J' & J & |\Delta J| \\ F & F' & I \end{matrix} \right\}^2 \sigma_{(K_a\sigma v_\tau)J \rightarrow (K'_a\sigma'v'_\tau)J'}. \quad (9)$$

To analyze which final hyperfine levels, F' , are mostly populated by (de-)excitation, we must sum equation (9) over all initial hyperfine states F . Then, we find for example for the collisional de-excitation $J = 6 \rightarrow J' = 5$ that the $F' = J' + 2$ state has a 14% higher propensity to be populated than the $F' = J' - 2$ state. The other hyperfine states with $F' = J'$ and $J' \pm 1$ are linear combinations of two nuclear spin states, and have population propensities lower than the $F' = J' + 2$ state and higher than $F' = J' - 2$ state.

Actually, one can also analyze the ratio between hyperfine rates including all L channels with equation (8), and find that hyperfine-state-specific collision propensities for the $F' = J' + 2$ state are even higher for the other L channels. We can therefore say that the hyperfine collisional de-excitation propensity is over 14% higher for the $F' = J' + 2$ state than for the $F' = J' - 2$ state. Hyperfine state specific collision rate propensities of intermediate F' states are somewhere between the two extremes. More in general, we find consistently that in collisional (de-)excitation, for $\Delta J < 0$ transitions, high F' states have a higher propensity for every L channel. In $\Delta J = 0$ transitions, there is no hyperfine preference, and in $\Delta J > 0$ transitions, low F' hyperfine states have the highest probability to be populated.

Hyperfine-state resolved radiative rates

To investigate which hyperfine transitions are favored by radiative de-excitation, we will recouple the line strength of a torsion-rotation transition to a hyperfine basis. From the line strength, one can easily compute the Einstein coefficient.

The line strength of a transition between torsion-rotation states $(K_a \sigma v_\tau)J$ and $(K'_a \sigma' v'_\tau)J'$ is

$$S_{(K_a \sigma v_\tau)J \rightarrow (K'_a \sigma' v'_\tau)J'} = \left| \sum_{MM'} \langle (K_a \sigma v_\tau)JM | \mathbf{d} | (K'_a \sigma' v'_\tau)J'M' \rangle \right|^2, \quad (10)$$

where \mathbf{d} stands for the total dipole moment vector of all charged particles, electrons and nuclei. In recoupling the rotational line strength to hyperfine-state specific line strengths, we recognize that the line strength transforms as a rank-1 tensor opacity, and we use equation (7) to obtain

$$S_{(K_a \sigma v_\tau)[JI]F \rightarrow (K'_a \sigma' v'_\tau)[J'I]F'} = [F][F'] \left\{ \begin{matrix} J' & J & 1 \\ F & F' & I \end{matrix} \right\}^2 S_{(K_a \sigma v_\tau)J \rightarrow (K'_a \sigma' v'_\tau)J'}. \quad (11)$$

The Einstein coefficient is related to the line strength by

$$A_{(K_a\sigma v_\tau)[JI]F \rightarrow (K'_a\sigma'v'_\tau)[J'I]F'} = \frac{2\omega^3}{3\epsilon_0 h c^3 [F]} S_{(K_a\sigma v_\tau)[JI]F \rightarrow (K'_a\sigma'v'_\tau)[J'I]F'}, \quad (12)$$

where ϵ_0 , h and c are the vacuum permittivity, Planck's constant, and the speed of light, respectively. ω is the transition frequency, which to a very good approximation does not depend on the hyperfine splittings of the rotational states.

To analyze which final hyperfine levels F' are mostly populated by (de-)excitation, we must sum equation (9) over all initial hyperfine states F : $A_{(K_a\sigma v_\tau)J \rightarrow (K'_a\sigma'v'_\tau)[J'I]F'}$. Then, we find for a $J = 6 \rightarrow J' = 5$ emission, for example, that the ratio between the Einstein coefficients for de-excitation to the final hyperfine states with $F' = J' + 2$ and $F' = J' - 2$ is

$$\frac{A_{(K_a\sigma v_\tau)6 \rightarrow (K'_a\sigma'v'_\tau)[5I]7}}{A_{(K_a\sigma v_\tau)6 \rightarrow (K'_a\sigma'v'_\tau)[5I]3}} = 1.14. \quad (13)$$

The intermediate hyperfine states with $F' = J'$ and $J' \pm 1$ are linear combinations of two nuclear spin states, and have population propensities lower than the $F' = J' + 2$ state and higher than the $F' = J' - 2$ state. The ratio calculated in equation (13) increases exponentially for lower J . For rotational states with higher J it decreases to 1.

DATA AVAILABILITY

The data that support the plots within this paper and other findings of this study are available from the corresponding author upon reasonable request.

CORRESPONDENCE

To whom correspondence should be addressed: Boy Lankhaar (boy.lankhaar@chalmers.se)

ACKNOWLEDGEMENTS

Support for this work was provided by the the Swedish Research Council (VR), and by the European Research Council under the European Union's Seventh Framework Programme (FP7/2007-2013), through the ERC consolidator grant agreement nr. 614264.

AUTHOR CONTRIBUTIONS

B.L., A.vd.A. and W.V. wrote the paper. B.L., A.vd.A. and G.C.G. modeled the Zeeman effect in methanol. B.L. and W.V. performed the analysis of the astrophysical maser spectra, based on methanol's Zeeman model. W.V., H.J.vd.L. and G.S. provided expertise on maser polarization in astrophysics and initiated the project. All authors discussed the results and commented on the manuscript.

COMPETING FINANCIAL INTERESTS

The authors declare no competing financial interests.

-
- [1] Crutcher, R. M. Magnetic fields in molecular clouds. *Annu. Rev. Astron. Astrophys.* **50**, 29–63 (2012).
 - [2] Vlemmings, W. H. T., Torres, R. M. & Dodson, R. Zeeman splitting of 6.7GHz methanol masers. *Astron. Astroph.* **529**, A95 (2011).
 - [3] Sarma, A. & Momjian, E. Detection of the Zeeman effect in the 36 GHz Class I CH₃OH maser line with the EVLA. *Astrophys. J. Lett.* **705**, L176 (2009).
 - [4] Sarma, A. & Momjian, E. Discovery of the Zeeman effect in the 44 GHz Class I methanol (CH₃OH) maser line. *Astrophys. J. Lett.* **730**, L5 (2011).
 - [5] Jen, C. K. Rotational magnetic moments in polyatomic molecules. *Phys. Rev.* **81**, 197 (1951).
 - [6] Lankhaar, B., Groenenboom, G. C. & van der Avoird, A. Hyperfine interactions and internal rotation in methanol. *J. Chem. Phys.* **145**, 244301 (2016).
 - [7] Baudry, A. & Diamond, P. VLBA polarization observations of the J= 7/2, 13.44 GHz OH maser in W3 (OH). *Astron. Astroph.* **331**, 697–708 (1998).
 - [8] Wright, M. M., Gray, M. D. & Diamond, P. J. The OH ground-state masers in W3(OH) II. Polarization and multifrequency results. *Mon. Not. R. Astron. Soc.* **350**, 1272–1287 (2004).
 - [9] Bagdonaite, J. *et al.* A stringent limit on a drifting proton-to-electron mass ratio from alcohol in the early universe. *Science* **339**, 46–48 (2013).

- [10] Kanekar, N. *et al.* Constraints on changes in the proton-electron mass ratio using methanol lines. *Mon. Not. R. Astron. Soc.* **448**, L104–L108 (2015).
- [11] Jansen, P., Xu, L.-H., Kleiner, I., Ubachs, W. & Bethlem, H. L. Methanol as a sensitive probe for spatial and temporal variations of the proton-to-electron mass ratio. *Phys. Rev. Lett.* **106**, 100801 (2011).
- [12] Daprà, M. *et al.* Testing the variability of the proton-to-electron mass ratio from observations of methanol in the dark cloud core I1498. *Mon. Not. R. Astron. Soc.* stx2308 (2017).
- [13] Engelbrecht, L. *Der Rotations-Zeemaneffekt bei Molekülen mit schwach behinderter interner Rotation*. Ph.D. thesis, University of Kiel (1975).
- [14] Deguchi, S. & Watson, W. D. Linearly polarized radiation from astrophysical masers due to magnetic fields when the rate for stimulated emission exceeds the Zeeman frequency. *Astrophys. J.* **354**, 649–659 (1990).
- [15] Vlemmings, W. H. T., Diamond, P. J., van Langevelde, H. J. & Torrelles, J. M. The magnetic field in the star-forming region Cepheus A. from H₂O maser polarization observations. *Astron. Astrophys.* **448**, 597–611 (2006).
- [16] Walker, R. H₂O in W49N. II-Statistical studies of hyperfine structure, clustering, and velocity distributions. *Astrophys. J.* **280**, 618–628 (1984).
- [17] Cragg, D., Sobolev, A. & Godfrey, P. Models of class II methanol masers based on improved molecular data. *Mon. Not. R. Astron. Soc.* **360**, 533–545 (2005).
- [18] Corey, G. & McCourt, F. R. Inelastic differential and integral cross sections for $^{2S+1}\sigma$ linear molecule-¹S atom scattering: the use of Hund’s case b representation. *J. Phys. Chem.* **87**, 2723–2730 (1983).
- [19] Surcis, G., Vlemmings, W. H. T., van Langevelde, H. J. & Hutawarakorn Kramer, B. EVN observations of 6.7 GHz methanol maser polarization in massive star-forming regions. *Astron. Astrophys.* **541**, A47 (2012).
- [20] Momjian, E. & Sarma, A. The Zeeman effect in the 44 GHz class I methanol maser line toward DR21 (OH). *Astrophys. J.* **834**, 168 (2017).
- [21] Crutcher, R. M. Magnetic fields in molecular clouds: observations confront theory. *Astrophys. J.* **520**, 706 (1999).
- [22] W. H. T. Vlemmings. A new probe of magnetic fields during high-mass star formation. *Astron. Astrophys.* **484**, 773–781 (2008).

- [23] Vlemmings, W., Surcis, G., Torstensson, K. & Van Langevelde, H. Magnetic field regulated infall on the disc around the massive protostar Cepheus A HW2. *Mon. Not. R. Astron. Soc.* **404**, 134–143 (2010).
- [24] Voronkov, M. A. *et al.* Class i methanol masers in the outflow of iras 16 547–4247. *Mon. Not. R. Astron. Soc.* **373**, 411–424 (2006).
- [25] Dall’Olio, D. *et al.* Methanol masers reveal the magnetic field of the high-mass protostar IRAS 18089-1732. *ArXiv e-prints* (2017). 1708.02961.
- [26] Marshall, M. A. *et al.* Methanol absorption in PKS B1830-211 at milliarcsecond scales. *Mon. Not. R. Astron. Soc.* **466**, 2450 (2017).
- [27] Xu, L.-H. *et al.* Torsion-rotation global analysis of the first three torsional states ($v_t = 0, 1, 2$) and terahertz database for methanol. *J. Mol. Spectr.* **251**, 305–313 (2008).
- [28] Jansen, P., Kleiner, I., Xu, L.-H., Ubachs, W. & Bethlem, H. L. Sensitivity of transitions in internal rotor molecules to a possible variation of the proton-to-electron mass ratio. *Phys. Rev. A* **84**, 062505 (2011).
- [29] Shinnaga, H. & Yamamoto, S. Zeeman effect on the rotational levels of CCS and SO in the $^3\sigma$ -ground state. *Astrophys. J.* **544**, 330 (2000).
- [30] Ramos, A. A. & Bueno, J. T. Theory and modeling of the Zeeman and Paschen-Back effects in molecular lines. *Astrophys. J.* **636**, 548 (2006).
- [31] Heuvel, J. & Dymanus, A. Hyperfine structure of CH₃OH. *J. Mol. Spectrosc.* **45**, 282 – 292 (1973).
- [32] Belov, S. P. *et al.* Torsionally mediated spin-rotation hyperfine splittings at moderate to high J values in methanol. *J. Chem. Phys.* **145** (2016).
- [33] Coudert, L., Gutlé, C., Huet, T., Grabow, J.-U. & Levshakov, S. Spin-torsion effects in the hyperfine structure of methanol. *J. Chem. Phys.* **143**, 044304 (2015).
- [34] Eshbach, J. R. & Strandberg, M. W. P. Rotational magnetic moments of closed shell molecules. *Phys. Rev.* **85**, 24–34 (1952).
- [35] Flygare, W. & Benson, R. The molecular zeeman effect in diamagnetic molecules and the determination of molecular magnetic moments (g values), magnetic susceptibilities, and molecular quadrupole moments. *Mol. Phys.* **20**, 225–250 (1971).
- [36] Sutter, D. & Flygare, W. The molecular Zeeman effect. In Craig, D., Mellor, D., Gleiter, R., Gygax, D., R. Sutter & Flygare, W. (eds.) *Bonding Structure. Topics in Current Chemistry*,

- vol. 63, 89–196 (Springer, Berlin, Heidelberg, 1976).
- [37] Flygare, W. Magnetic interactions in molecules and an analysis of molecular electronic charge distribution from magnetic parameters. *Chem. Rev.* **74**, 653–687 (1974).
- [38] Gauss, J., Ruud, K. & Helgaker, T. Perturbation-dependent atomic orbitals for the calculation of spin-rotation constants and rotational g-tensors. *J. Chem. Phys.* **105**, 2804 (1996).
- [39] Lutnaes, O. B. *et al.* Benchmarking density-functional-theory calculations of rotational g tensors and magnetizabilities using accurate coupled-cluster calculations. *J. Chem. Phys.* **131**, 144104 (2009).
- [40] Stanton, J., Gauss, J., M.E., H. & Szalay, P. CFOUR, Coupled-Cluster techniques for Computational Chemistry. [Http://www.cfour.de](http://www.cfour.de).
- [41] Dunning Jr, T. H. Gaussian basis sets for use in correlated molecular calculations. I. The atoms boron through neon and hydrogen. *J. Chem. Phys.* **90**, 1007–1023 (1989).
- [42] Engelbrecht, L., Sutter, D. & Dreizier, H. Zeeman effect of molecules with low methyl barriers. I. Nitromethane. *Z. Naturforsch. A* **28**, 709–713 (1973).
- [43] Mulliken, R. S. Electronic population analysis on LCAO-MO molecular wave functions. I. *J. Chem. Phys.* **23**, 1833–1840 (1955).
- [44] Alexander, M. H. & Dagdigian, P. J. Collision-induced transitions between molecular hyperfine levels: Quantum formalism, propensity rules, and experimental study of $\text{CaBr}(X^2\sigma_+) + \text{Ar}$. *J. Chem. Phys.* **83**, 2191–2200 (1985).
- [45] Neufeld, D. A. & Green, S. Excitation of interstellar hydrogen chloride. *Astrophys. J.* **432**, 158–166 (1994).
- [46] Davis, S. L. Torsionally inelastic collisions between a near-symmetric top molecule and a structureless atom. *J. Chem. Phys.* **95**, 7219–7225 (1991).

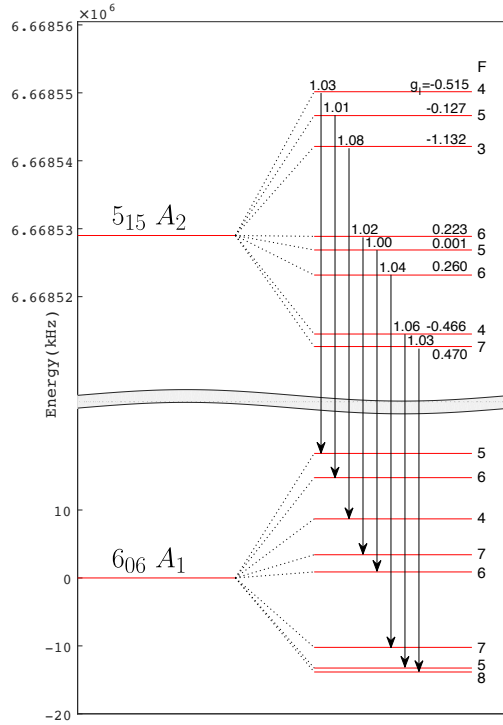


FIG. 1: Hyperfine structure of the torsion-rotation levels in the 6.7 GHz ($5_{15} A_2 \rightarrow 6_{06} A_1$) transition. The energy of the $6_{06} A_1$ torsion-rotation level is set to zero. Because hyperfine interactions (≈ 10 kHz) are much smaller than the torsion-rotation energy difference (≈ 10 GHz), we have broken the y-axis. Torsion-rotation states of A -symmetry have nuclear spin quantum numbers $I = 1$ and 2 , so that for rotational states with $J \geq 2$ there are six levels with $F = J, J \pm 1$ and two levels with $F = J \pm 2$, each $2F + 1$ -fold degenerate. Hence, the $F = J, J \pm 1$ states contain both $I = 1$ and $I = 2$ components which are mixed[6]. The hyperfine structure of the torsion-rotation levels is ≈ 30 kHz wide. Arrows indicate the strongest hyperfine transitions with $\Delta F = \Delta J = 1$, with the Einstein A-coefficients (in 10^{-9} s^{-1}) indicated above. Landé g-factors of the transitions in a magnetic field of 10 mG are given at the righthand side of the upper energy levels. The rightmost numbers are the F quantum numbers of the hyperfine states.

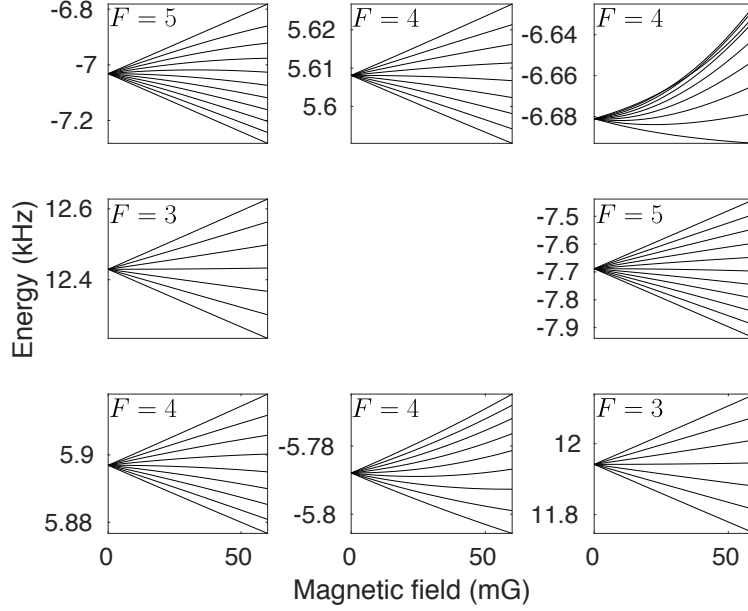


FIG. 2: Splitting of the 8 hyperfine levels of the torsion-rotation $4_{-1} E$ state as a function of the magnetic field strength. The quantum number F of each hyperfine level is given in the upper lefthand corner. In a magnetic field each hyperfine level splits into $2F + 1$ magnetic substates. The energy on the vertical axis is defined relative to the energy of the corresponding torsion-rotation state $4_{-1} E$.

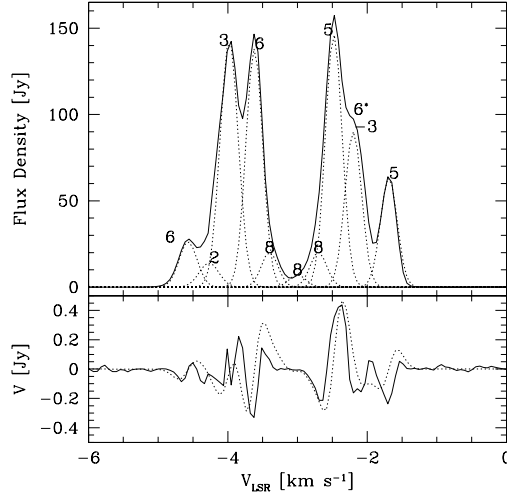


FIG. 3: Total intensity (flux density in $\text{Jy} = 10^{-26} \text{ W m}^{-2} \text{ Hz}^{-1}$) and circular polarization (V) spectra of the 6.7 GHz ($5_{15} A_2 \rightarrow 6_{06} A_1$) methanol masers around the disc of the high-mass protostar Cepheus A HW2[23]. The spectra were observed with the Effelsberg 100-m telescope. They originate from methanol masers with different velocities along the same line of sight and can be approximated by ten Gaussian peaks. If we assume that a single hyperfine component is dominant, our calculations imply an average line-of-sight magnetic field strength $B_{\parallel} = 7.7 \pm 1.0$ mG. The field strengths (in mG) extracted from the individual components, with errors of $\approx 20\%$, are indicated in the figure. This corresponds to a total magnetic field strength of $|B| = 26$ mG. In one of the peaks the maser radiation is polarized in the opposite direction than in the other peaks, which seems to indicate a reverse magnetic field. We argue, however, that this could be due to pumping of a different hyperfine component with a different Landé g -factor. When this argument holds, the magnetic field (denoted with the asterisk) extracted from this component has the same direction and is of similar magnitude as the fields from the other maser components. Using information on the masing gas and the mass of the region where the magnetic field is probed[23], the recalculated ratio of $\beta = 0.2$ between the thermal and magnetic energy shows the dominance of the magnetic field. The recalculated mass to magnetic flux ratio compared to the critical ratio is $\lambda = 1.5$.